https://doi.org/10.48048/tis.2022.5101

An Optimized Model of Single Phase Self Excited Induction Generator

Gurdiyal Singh[1,*] and Ved Ram Singh[2]

[1]University Institute of Engineering & Technology, Maharshi Dayanand University, Rohtak, Haryana 124001, India
[2]PDM College of Technology & Management, Bahadurgarh, Haryana 124507, India

([*]Corresponding author's e-mail: gurdiyal.malik@gmail.com)

Received: 10 December 2020, Revised: 24 July 2021, Accepted: 10 August 2021

Abstract

This paper illustrates the newly developed specially designed single phase self excited induction generator. All possible configurations for winding arrangement have been attempted to obtain the best output from the model. The earlier configurations were found incomplete to obtain the optimum output from the single phase induction machine as an induction generator. The proposed model is unified, optimum and accurate for inculcating the performance of single phase induction generator. The model design as well as its development of 3.7 kW, 50 Hz and 4-pole single phase SEIG is presented using simulink in MATLAB. The 4 possible configurations are designed for single phase SEIG, the objective function is to reduce total harmonic distortion (THD) and optimize the model parameter. The results were demonstrated experimentally validated using SPEED software. A standard available IEC 132 frame size is used for development of proposed model and the results found are prominent.

Keywords: Single-phase self-excited induction generator (SEIG), Design and development, Capacitor self-excitation, Matlab, Autonomous power generation, Total harmonic distortion

Introduction

The non-conventional energy sources are going to be depleted increasingly day by day, based on a survey the oil will be reach low level in about 40 years and the coal reserves will be depleted in about 120 years. Therefore, the new millennium belongs to renewable energy sources [1-6]. Sometimes in rural and remote areas, where it is difficult to install the transmission and distribution line, for such an areas SEIG is found to be suitable for power generation from such renewable energy sources due to its inherent advantages [7] such as low cost, simple construction, little maintenance, absence of dc source, brushless etc compared to conventional generator.

An Induction machine can be made to work as a self excited generator. When the rotor of an induction machine is driven by a prime mover and its excitation is provided by connecting a capacitor across the stator terminals. The induced emf and current in the stator winding will continue to rise until equilibrium is attained due to magnetic saturation in the machine.

A breakthrough was achieved by evolving a specially designed 2 winding single phase SEIG with a self regulating capacitor topology [8] which has been recognised by Boldea as the most acceptable single phase SEIG. But it is observed that there is a heavy demand for small capacity generator in rural sector. In this paper the work is reported for the optimised model for such a need. Mostly generators are operating at near 1,500 rpm. Hence a 4-pole configuration of single phase SEIG is chosen.

This paper reports a successful effort on the design and development of a 3.7 kW, 50Hz, 230 V, 4-pole single-phase 2 winding self excited induction generator (SEIG). Since such an exercise is taken first time with design and its optimised model is implemented. The author has taken the reference based on this optimised result, a prototype was implemented in the lab using standard IEC 132 frame and tested for suitability.

Design modelling of self-excited induction generator

Here 2 winding single phase 230V output power of 3.7KW with 50 Hz frequency and 4-poles operating as SEIG is presented. The excitation in both systems is caused by residual flux activation, which is in stator torque, when the rotor is excited by a mild EMF. The approach taken is acceptable and will be briefly outlined here. A normal single-phase motor cannot be used satisfactorily as a self-excited induction based on experience, while the development goal of a single-phase good start and run output with high efficiency and power factor [25]. There are usually multiple steps included in a development process for a SEIG. The induction generator variable measurements were carried out using theoretical and statistical formulas. Figure 1 demonstrates the planned treatment.

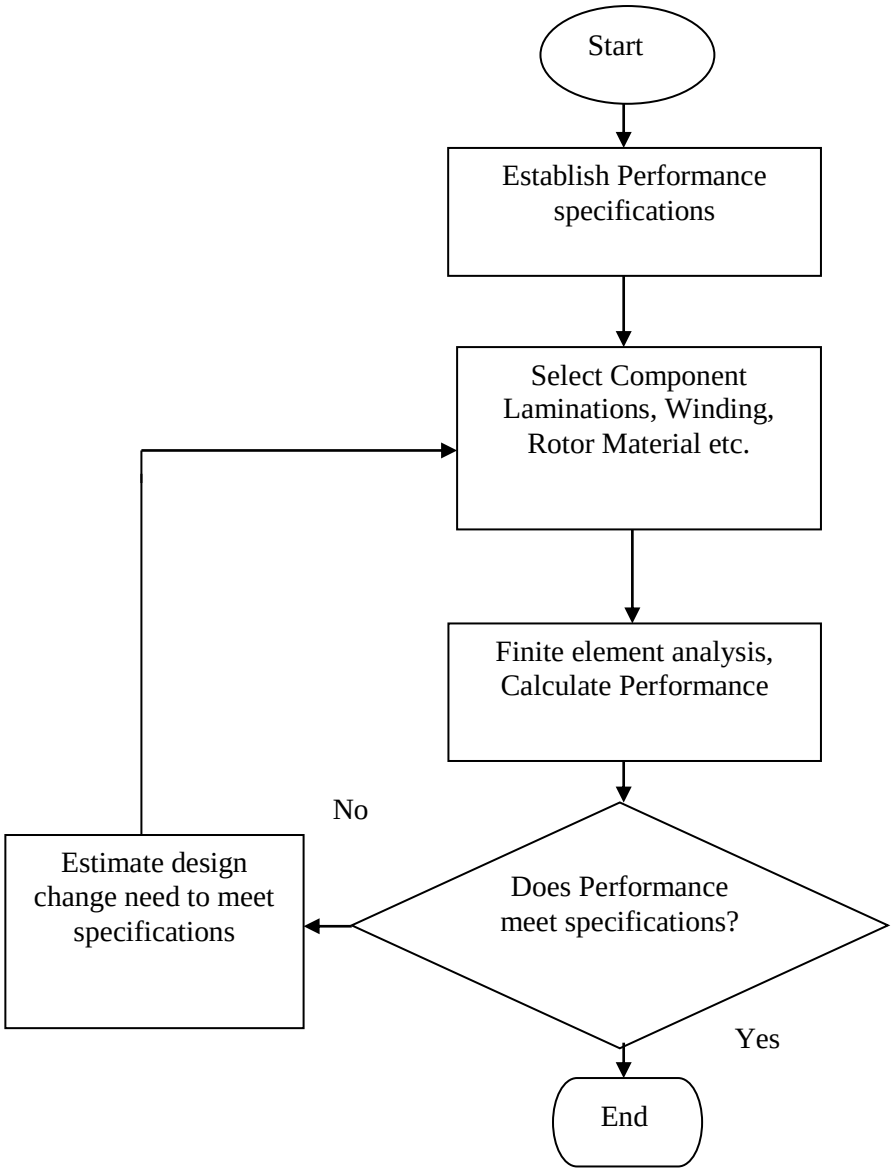

Figure1 Design system for proposed SEIG.

AC machine's performance are expressed by formula (1),

$$S = C_0 D^2 L * n_s \quad (1)$$

where,

$$C_o = 1.1\pi^2 B_{av} ACK_w * 10^{-3} \tag{2}$$

The KVA input of generator is S. The coefficient of output is C_o. The average flux density in the air-gap is B_{av}. The specific electric loading is AC. The air-gap diameter is D. The core length is represented as L and the synchronous speed is represented as n_s. The winding factor is represented as K_w. Regarding rated output power (P_0), efficiency (η) and power factor. The KVA input (S) is determined as,

$$S = \frac{P_0}{\eta \cos\phi} \tag{3}$$

where, the main parameters for the structure of the SEIG are named qualities because they are recognized as B_{av} and AC. SEIG can work in the enrichment region [26] when selecting a higher value B_{av}. The operating point may be in the sinking zone when a SEIG is in the load position. Then, the current waveform is not sinusoidal for the misalignment of the magnetic flux. Flux for a pole,

$$\phi = \alpha_i \tau L_i B_{av} \tag{4}$$

where pole pitch is represented as τ, Net core iron is represented as L_i.

The performance of the teeth is referred to as the flux density to the magnetic saturation is represented as α_i.

The SEIG operating point in the perimeter region causes flux density enrichment in the teeth. Thus, making the stator size a point N_s is given.

$$N_s = \frac{E_g}{4K_f \phi f K_w} \tag{5}$$

where, the inductance voltage is represented as E_g, the frequency is represented as f and the structure factor subject to teeth saturation is represented as K_f which 1.02<<1.11.

In enhancement, the advanced voltage of the SEIG is a sinusoidal waveform, which means better power efficiency and lower voltage control. The rotor winding includes conductors proportional to the poles' tendency of the SEIG. The explanation behind tilting the rotor is proportional to rotating the stator. The winding segment (K_w) is shown as,

$$K_w = K_d K_P K_{sk} \tag{6}$$

where,the distribution factor is denoted as K_d ,the pitch factor is represented as K_p and the skew factor is signified as K_{sk}. The rated current can be obtained as,

$$I_g = \frac{P_0}{3\eta V_t \cos\phi} \tag{7}$$

The cross-section area of the stator conductor is represented as (a_s),

$$a_s = \frac{I_g}{\delta_s} \tag{8}$$

where is the current density of the stator conductors. The current of the rotor is the current of the rotor bar. Rotor bar current,

$$I_b = \frac{2mK_w N_s}{N_2} I_s \cos\phi \tag{9}$$

where, the number of the phase is taken as m. As the sum of the average bar current and the half bar per pole per phase, this obtains the largest estimate of what is done with the ring current. The rms estimate of the final loop current (for example, the root mean square value or the value used to break the alternating current circuits) is thus obtained,

$$I_{er} = \frac{N_2 I_b}{\pi\rho} \tag{10}$$

The flux density of the teeth is not more important than the normal degrees of the magnetic field of the selected object. The motion of the stator and rotor is given as follows.

$$B_{ts} = \frac{\phi}{\frac{N_1}{\rho} L_i W_{ts}} \tag{11}$$

$$B_{tr} = \frac{\phi}{\frac{N_2}{\rho} L_i W_{tr}} \tag{12}$$

where the stator tooth width is represented as W_{ts} and the rotor tooth is represented as W_{tr}, respectively.

Single phase 2 winding SEIG model

Figure 2 shows the Schematic of 1-Phase 2 winding SEIG. The most significant single phase SEIG with one as the main winding through which load is connected and the other is the auxiliary winding through which capacitor is connected to provide the excitation. In this process the design of 2 winding is taken for 36 slots, 4 poles for stator core and the squirrel cage rotor are kept unaltered.

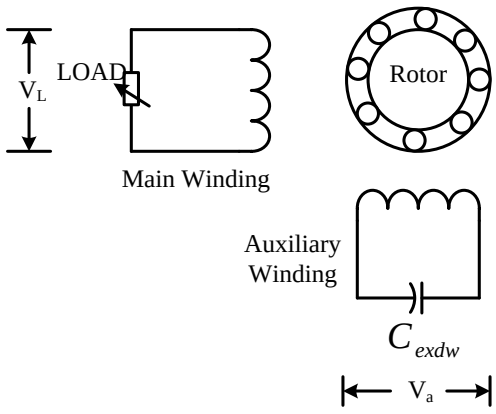

Figure2 Schematic of 1-phase 2 winding SEIG.

The steady state circuit of a single phase 2-winding SEIG is shown in **Figure 3**. It generally represents the equivalent circuit of a single phase induction motor in generation mode of operation and is derived from double revolving field theory.

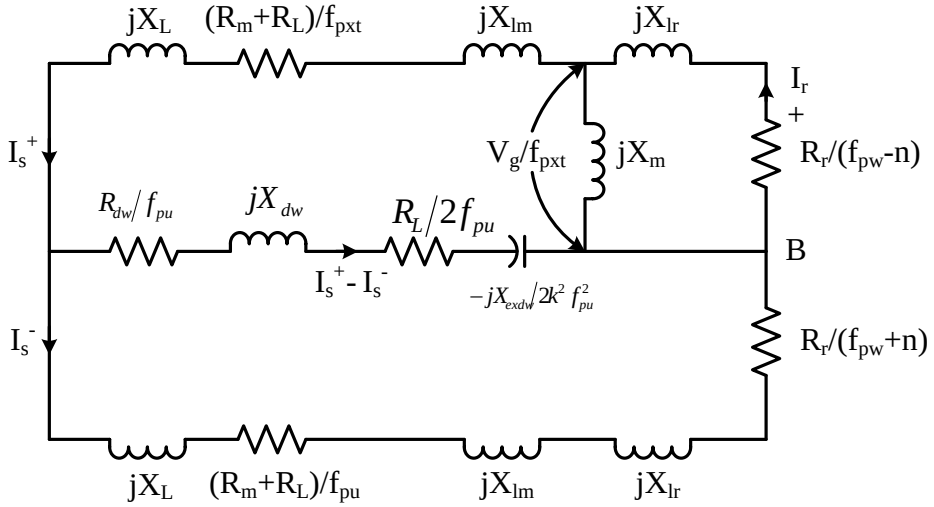

Figure3 Steady state circuit model of a single phase 2 winding SEIG.

The equations derived for its performance evaluation based on its circuit model are as follows:

$$Z_1 = \left(R_{in} + R_L\right)/\, f_{pu} + j\left(X_{\mathrm{Im}} + X_L\right) \tag{13}$$

$$Z_2 = \frac{R_a}{k^2 f_{pu}} + j\left(\frac{X_{la}}{k^2}\right) - j\frac{X_{exdw}}{k^2 f_{pu}^2} \tag{14}$$

$$Z_{dw} = \frac{R_{dw}}{f_{pu}} + jX_{dw} = \left(z_2 - z_1\right)/2 \tag{15}$$

Where,

$$\left.\begin{aligned} R_{dw} &= \left(R_a/k^2 - R_m\right)/2 \\ X_{dw} &= \left(X_{la}/k^2 - X_{lm}\right)/2 \end{aligned}\right\} \tag{16}$$

$$Z_T^- = \frac{R_r}{\left(f_{pu} + n\right)} + jX_{lr} \tag{17}$$

$$Z_s^- = Z_1 + Z_T^- \tag{18}$$

$$Z_{comb} = Z_1 + \left[\frac{\left(Z_s^- * Z_{dw}\right)}{\left(Z_s^- + Z_{dw}\right)}\right] \tag{19}$$

$$= R + jX \tag{20}$$

$$I_s^+ = \frac{V_g / f_{pu}}{Z_{comb}} \tag{21}$$

$$I_s^- = \left(I_s^+ * Z_{dw}\right) / Z_s^- + Z_{dwd} \tag{22}$$

$$I_T^+ = -\frac{V_g / f_{pu}}{Z_T^+} \tag{23}$$

$$Z_T^+ = \frac{R_T}{\left(f_{pu} - n\right)} + jX_{lr} \tag{24}$$

$$I_m = I_{L.DW} = I_s^+ + I_s^- \tag{25}$$

$$I_a = \frac{j\left(I_s^+ - I_s^-\right)}{k} \tag{26}$$

$$V_L = I_m\left(\left(R_L / f_{pu}\right) + jX_L\right) \tag{27}$$

$$V_a = I_a^*\left(\frac{X_{exdw}}{f_{pu}}\right) \tag{28}$$

$$P_{out} = I_m^2 * R_L \tag{29}$$

$$Z_{eq} = Z_{comb} + \frac{jX_m\left[R_r / \left(f_{pu} - n\right) + jX_{lr}\right]}{\left[R_r / \left(f_{pu} - n\right) + j\left(X_m + X_{lr}\right)\right]} \tag{30}$$

$$= R_{eq} + jX_{eq} \tag{31}$$

Equivalent circuit analysis

To create a broader view of the impact of the capacitor on the device with essential VAR compensation control, the proposed computer research divides the capacitors into 2 parts called the voltage-generator to compensate for the terminal voltage regulator. The recommended model is shown in **Figure 4(a)**.

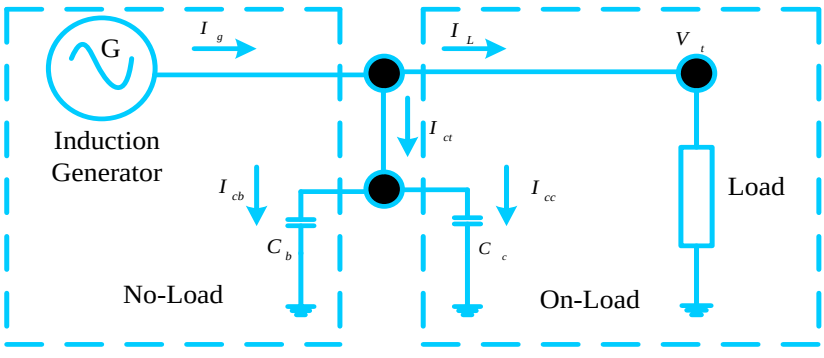

(a)

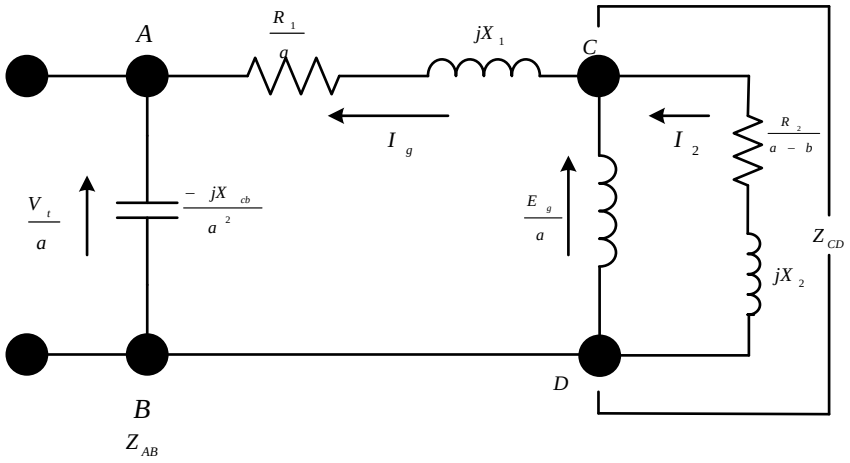

(b)

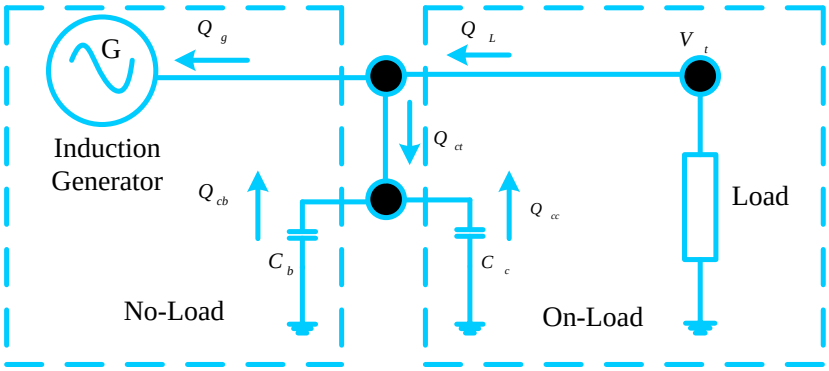

(c)

Figure 4 Analysis of (a) Single line outline of SEIG (b) Power stream chart of SEIG without loading a phase proportional circuit of SEIG.

Equal circuit for each phase is shown in **Figure 4(b)** for no load operation, neglect harmonic effect and core loss. It is possible to determine the capacitance for the process of voltage building during no load as,

$$C_b = \frac{1}{\left\{2\pi f_b Z_b a_{\max}^2 \left(X_1 + X_{CD}\right)\right\}} \tag{32}$$

Where,

$$a_{\max} = b - \frac{b}{2}\left[\frac{1-\sqrt{1-\left(\frac{b_c}{b}\right)^2}}{1+\left(\frac{R_1}{R_2}\right)\left(1+\frac{X_2}{X_m}\right)^2}\right] \tag{33}$$

$$b_c = \frac{2R_1}{X_m}\sqrt{\frac{R_2}{R_1}+\left(1+\frac{X_2}{X_m}\right)^2} \tag{34}$$

Each phase voltage is denoted by C_b capacitance, the fundamental impedance Z_b, f_b is denoted as the fundamental frequency, $a_{\max}$ is the coefficient is denoted, and the critical speed is denoted by b_c. To succeed in constructing the SEIG voltage, the terminal voltages must be controlled while the load C_c is increased. Digits are included to evaluate the load process. The energy stream characteristic of the SEIG that gives the load resistance is seen in **Figure 4(c)**. Calculate the terminal voltage as a constant C_c and find it. Condition (35) measures the total reactive power of the capacitors (for example, and

$$Q_{ct} = Q_g + Q_L \tag{35}$$

Here,

$$Q_L = 0 \tag{36}$$

$$Q_g = \sqrt{S_g^2 - P_g^2} = I_g^2 x_1 + I_\phi^2 x_m + I_2^2 x_2 \tag{37}$$

where,

The apparent power of a phase SEIG is represented as S_g, The Active power of the SEIG of a phase is represented as P_g ,The Reactive power of the SEIG of a phase is represented as Q_g ,The Reactive power load of a phase is represented as Q_L ,The Total reactive power of capacitors of a phase is represented as Q_{ct}.

The compensated reactive power is,

$$Q_{cc} = Q_{ct} - Q_{cb} \tag{38}$$

Where,

$$Q_{cb} = 2\pi \frac{V_t^2}{a}\left(fC_b\right) \tag{39}$$

The Reactive power of the voltage build-up capacitor of a phase is represented as Q_{cb}, The Reactive power of the compensating capacitor of a phase is represented as Q_{cc}.

The compensating capacitor's per-phase current is determined by equation (40).

$$I_{cc} = \frac{Q_{cc}}{V_t \diagup a} \tag{40}$$

The following equations measure the per-phase compensated capacitance.

$$X_{cc} = \frac{V_t / a}{I_{cc}} \tag{41}$$

$$C_c = \frac{1}{2\pi f\left(jX_{cc}\right)} \tag{42}$$

Therefore the overall SEIG capacitor value is,

$$C_t = C_b + C_c \tag{43}$$

Where,

The per-phase compensating capacitance is represented as C_c, The per-phase voltage build-up capacitance is represented as C_b, The per-phase total capacitance is represented as C_t.

Various configuration and model of 1-phase SEIG

Using the standard stamping details and software, design calculations are carried out for the following 4 possible winding models and presented in sections to follow. All possible configurations have been attempted and the performance also compared. Since the software gives only the motor performance the same is presented although we have to separately compute SEIG performance from parameters as discussed below;

Model 1: Full pitch(1-10) single layer winding
Model 2: Full pitch(1-10) double layer winding
Model 3: Short pitch(1-8) double layer winding
Model 4: Short pitch(1-9) double layer winding

Model 1: Full pitch(1-10) single layer winding

Table 1 represents the configuration for full pitch (1-10), Single layer winding for Main and auxiliary as phase-1 and phase-2. In this model the coil span is 9 and the number of turns are taken as 50.

Table 1 Winding details for main and auxiliary.

Phase-1 (Main)					Phase-2 (Aux)				
Coil	Go	Return	Span	Turns	Coil	Go	Return	Span	Turns
1	1	10	9	50	1	6	15	9	50
2	2	11	9	50	2	7	16	9	50
3	3	12	9	50	3	8	17	9	50
4	4	13	9	50	4	9	18	9	50
5	5	14	9	50	5	24	33	9	50
6	19	28	9	50	6	25	34	9	50
7	20	29	9	50	7	26	35	9	50
8	21	30	9	50	8	27	36	9	50
9	22	31	9	50					
10	23	32	9	50					

Table 2 represents the configuration for full pitch (1-10), Single layer winding for Main and auxiliary as phase-1 and phase-2 for all phases. In this model the coil span is 9 and the number of turns are taken 50. The coil span factor is 0.39 and 0.58.

Table 2 Winding details for main and auxiliary with slot fill factor.

Slot	Ph-1	Ph-2	Total	SFg	SFn	Slot	Ph-1	Ph-2	Total	SFg	SFn
1	50	0	50	0.3984	0.5889	19	50	0	50	0.3984	0.5889
2	50	0	50	0.3984	0.5889	20	50	0	50	0.3984	0.5889
3	50	0	50	0.3984	0.5889	21	50	0	50	0.3984	0.5889
4	50	0	50	0.3984	0.5889	22	50	0	50	0.3984	0.5889
5	50	0	50	0.3984	0.5889	23	50	0	50	0.3984	0.5889
6	0	50	50	0.3984	0.5889	24	0	50	50	0.3984	0.5889
7	0	50	50	0.3984	0.5889	25	0	50	50	0.3984	0.5889
8	0	50	50	0.3984	0.5889	26	0	50	50	0.3984	0.5889
9	0	50	50	0.3984	0.5889	27	0	50	50	0.3984	0.5889
10	-50	0	50	0.3984	0.5889	28	-50	0	50	0.3984	0.5889
11	-50	0	50	0.3984	0.5889	29	-50	0	50	0.3984	0.5889
12	-50	0	50	0.3984	0.5889	30	-50	0	50	0.3984	0.5889
13	-50	0	50	0.3984	0.5889	31	-50	0	50	0.3984	0.5889
14	-50	0	50	0.3984	0.5889	32	-50	0	50	0.3984	0.5889
15	0	-50	50	0.3984	0.5889	33	0	-50	50	0.3984	0.5889
16	0	-50	50	0.3984	0.5889	34	0	-50	50	0.3984	0.5889
17	0	-50	50	0.3984	0.5889	35	0	-50	50	0.3984	0.5889
18	0	-50	50	0.3984	0.5889	36	0	-50	50	0.3984	0.5889

Model 3: Short pitch(1-8) double layer winding

Table 3 represents the configuration for short pitch (1-8), Double layer winding for Main and auxiliary as phase-1 and phase-2. In this model the coil span is 7 and the number of turns are taken 25.

Table 3 Winding details for main and auxiliary (**Model 3**).

Phase-1 (Main)					Phase-2 (Aux)				
Coil	Go	Return	Span	Turns	Coil	Go	Return	Span	Turns
1	1	8	7	25	1	13	6	-7	25
2	2	9	7	25	2	14	7	-7	25
3	3	10	7	25	3	15	8	-7	25
4	4	11	7	25	4	16	9	-7	25
5	5	12	7	25	5	15	22	7	25
6	17	10	-7	25	6	16	23	7	25
7	18	11	-7	25	7	17	24	7	25
8	19	12	-7	25	8	18	25	7	25
9	20	13	-7	25	9	31	24	-7	25
10	21	14	-7	25	10	32	25	-7	25
11	19	26	7	25	11	33	26	-7	25
12	20	27	7	25	12	34	27	-7	25
13	21	28	7	25	13	33	4	7	25
14	22	29	7	25	14	34	5	7	25
15	23	30	7	25	15	35	6	7	25
16	35	28	-7	25	16	36	7	7	25
17	36	29	-7	25					
18	1	30	-7	25					
19	2	31	-7	25					
20	3	32	-7	25					

Table 4 represents the configuration for short pitch (1-8), Double layer winding for Main and auxiliary as phase-1 and phase-2 for all phases. In this model the coil span is 7 and the number of turns are taken 50. The coil span factor is 0.44 and 0.66, respectively.

Table 4 Winding details for main and auxiliary with slot fill factor (**Model 3**).

Slot	Ph-1	Ph-2	Total	SFg	SFn	Slot	Ph-1	Ph-2	Total	SFg	SFn
1	50	0	50	0.4407	0.6601	19	50	0	50	0.4407	0.6601
2	50	0	50	0.4407	0.6601	20	50	0	50	0.4407	0.6601
3	50	0	50	0.4407	0.6601	21	50	0	50	0.4407	0.6601
4	25	-25	50	0.4407	0.6601	22	25	-25	50	0.4407	0.6601
5	25	-25	50	0.4407	0.6601	23	25	-25	50	0.4407	0.6601
6	0	-50	50	0.4407	0.6601	24	0	-50	50	0.4407	0.6601
7	0	-50	50	0.4407	0.6601	25	0	-50	50	0.4407	0.6601
8	-25	-25	50	0.4407	0.6601	26	-25	-25	50	0.4407	0.6601
9	-25	-25	50	0.4407	0.6601	27	-25	-25	50	0.4407	0.6601
10	-50	0	50	0.4407	0.6601	28	-50	0	50	0.4407	0.6601
11	-50	0	50	0.4407	0.6601	29	-50	0	50	0.4407	0.6601
12	-50	0	50	0.4407	0.6601	30	-50	0	50	0.4407	0.6601
13	-25	25	50	0.4407	0.6601	31	-25	25	50	0.4407	0.6601
14	-25	25	50	0.4407	0.6601	32	-25	25	50	0.4407	0.6601
15	0	50	50	0.4407	0.6601	33	0	50	50	0.4407	0.6601
16	0	50	50	0.4407	0.6601	34	0	50	50	0.4407	0.6601
17	25	25	50	0.4407	0.6601	35	25	25	50	0.4407	0.6601
18	25	25	50	0.4407	0.6601	36	25	25	50	0.4407	0.6601

Winding configuration

These are the winding diagram in figure no. 4(d) of the finalised model taken during the design procedure in the design package/tool SPEED.

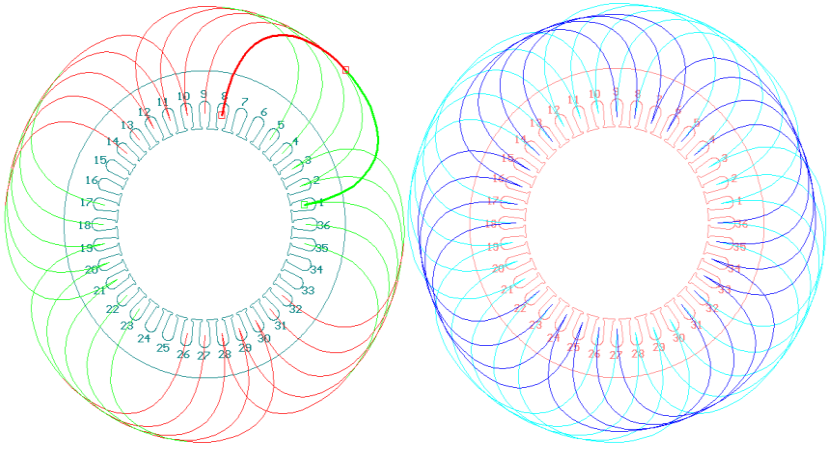

(d)

Figure 4 (d) Winding diagram of finalised model.

Results and discussion

Since the induction machine operates in SEIG mode, the differences in terminal voltage and current are evaluated. This paper is carried out using induction generator design analysis. In MATLAB / Simulink mode, the dynamic design of the proposed system is developed and the simulated system output is introduced. This section demonstrates the development of the simulated voltage waveform during normal SEIG operation, auxiliary torque voltage, generator voltage, motor rate and load, end-voltage and total harmonic distortion analysis (THD). **Figure 5** shows a simulink model of a 2-phase 4-pole SEIG of a grid.

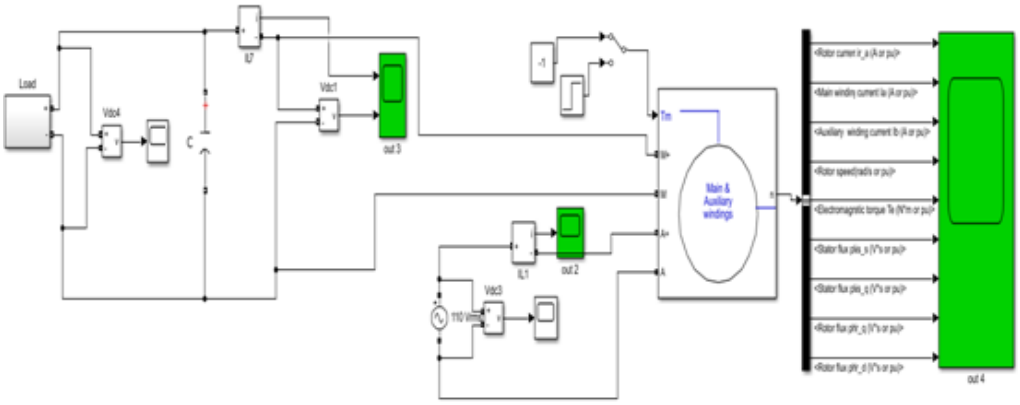

Figure 5 Simulink model of proposed methodology.

The response and the variation in the main and the auxiliary winding current are examined by simulation. The variation in the stator flux is also plotted. The effect of rotor resistance on kinetic energy has been tested for 2 different values of kinetic energy. Analysis of the main winding current is shown in **Figure 6(a)**, where the value of the current starts at 0 and slowly rises to 1.3A. The auxiliary value is illustrated with the 12A current representing in **Figures 6(b) - 6(d)** shows the stator flow of 1.7and 1.75wb on the d and q axis.

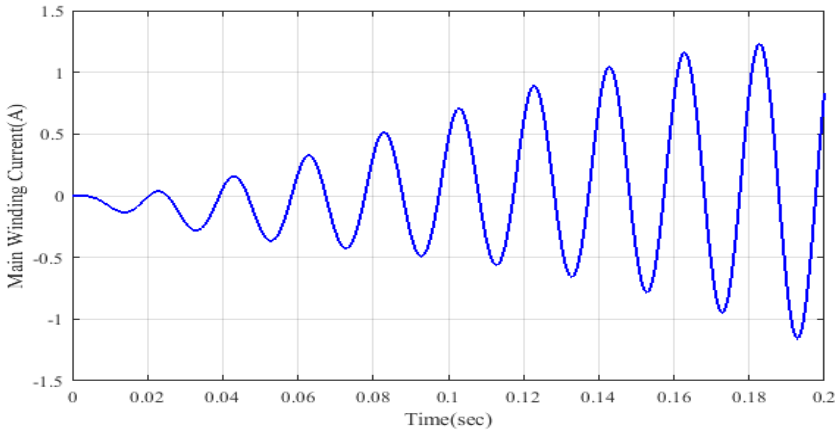

Figure 6(a) Analysis of Main winding current.

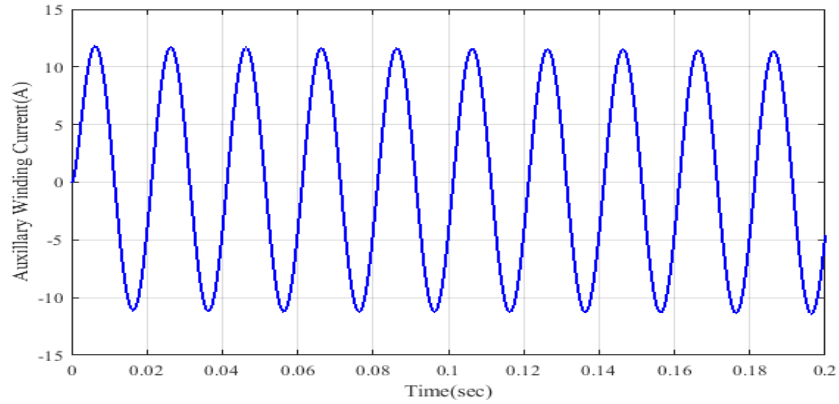

Figure 6(b) Analysis of auxiliary winding current.

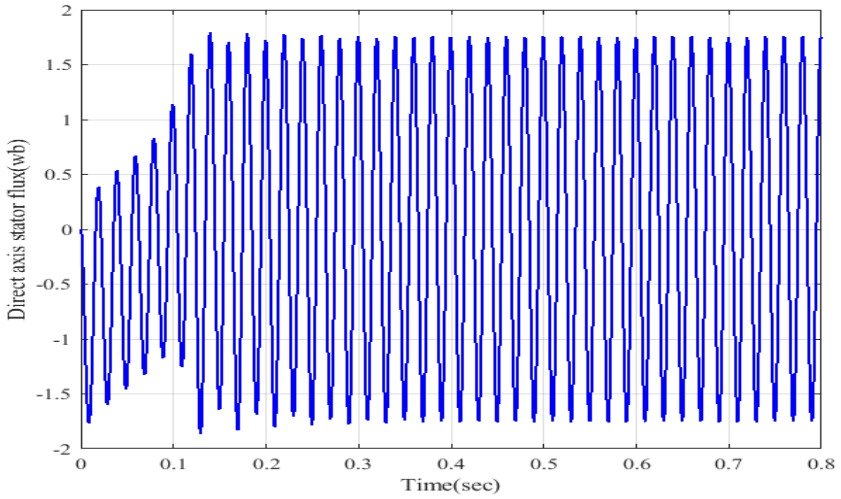

Figure 6(c) Analysis of stator flux at d-axis.

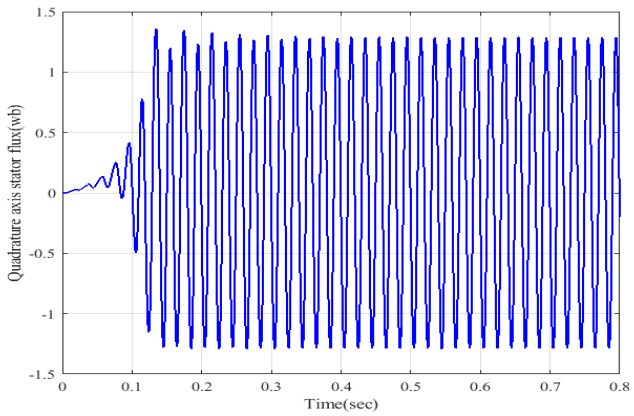

Figure 6(d) Analysis of stator flux at q-axis.

The response for the rotor parameters are presented in this section. Various graph shows the rotor performances in terms of speed, flux and current. **Figure 7(a)** illustrates the current waveform with value 48A. Rotor flux at d axis is 1.7wb and at q axis is 1.75wb, which is shown in **Figures 7(b)** and **7(c)**, respectively. **Figure 7(d)** shows the abruptly increasing the rotor speed to 89 rpm from 0.

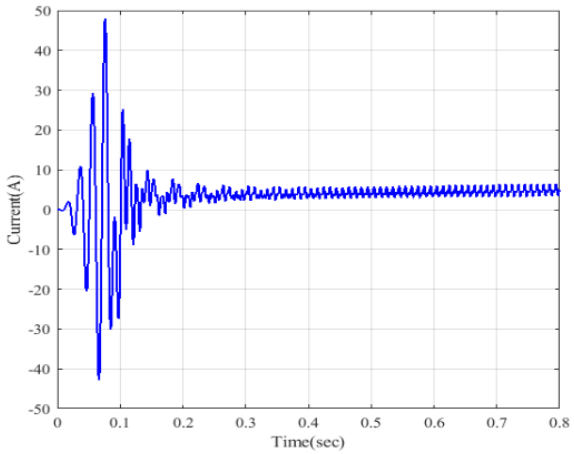

Figure 7(a) Analysis of Rotor current.

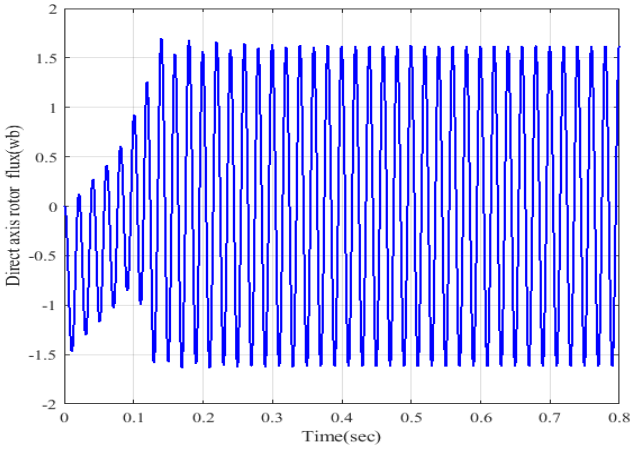

Figure 7(b) Analysis of rotor flux at d-axis.

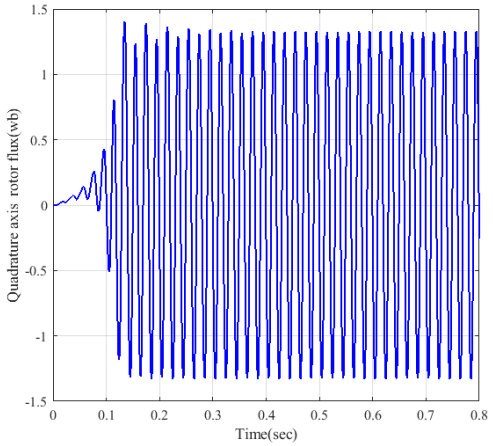

Figure 7(c) Analysis of rotor flux at q-axis.

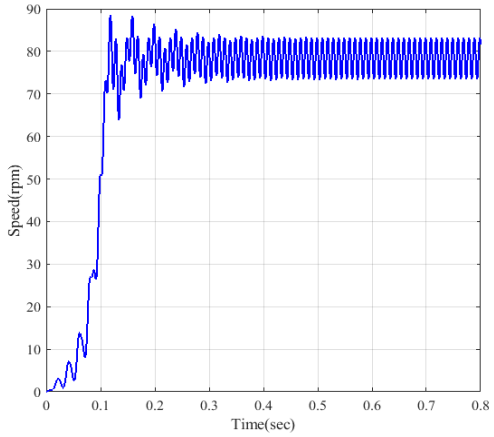

Figure 7(d) Analysis of rotor speed.

The generating voltage depends on the machine rating, frequency and connected capacitor to the terminal. **Figure 8(a)** shows the load current at 4A and the voltage rises for a period of 0.8 s and **Figure 8(b)** shows the load voltage. **Figure 8(c)** illustrates the power waveform and the power value at 0-0.1 s is the same after 0.3, which gradually rises and reaches 1,690 W. The electromagnetic torque of 75 Nm is shown in **Figure 8(d)**.

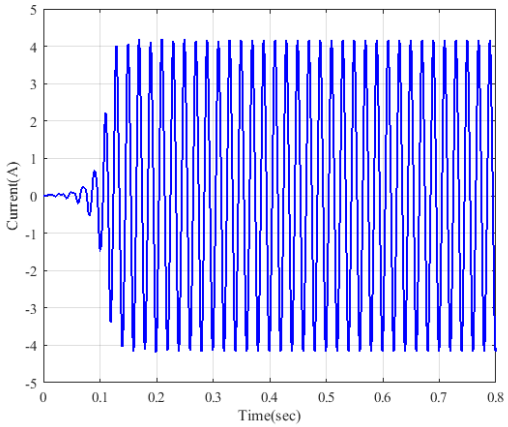

Figure 8(a) Analysis of load current.

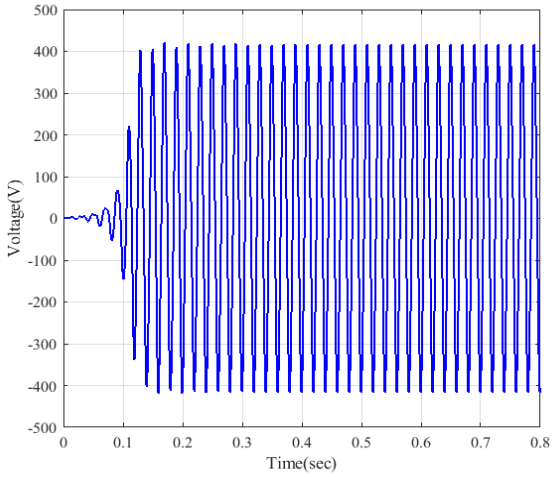

Figure 8(b) Analysis of load voltage.

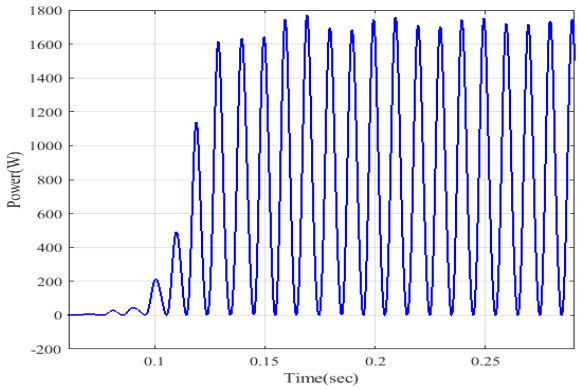

Figure 8(c) Analysis of load power.

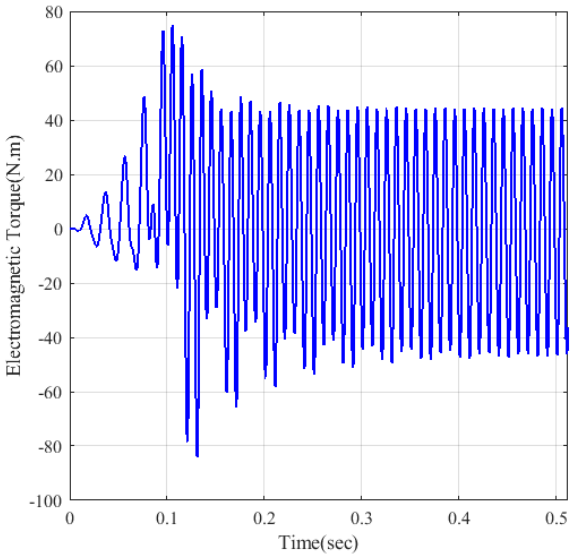

Figure 8(d) Analysis of electromagnetic torque.

The waveform of single phase SEIG for stator and rotor are displayed in **Figures 6** and **7** likewise the performance of THD response is given in **Figure 9**. The THD value of this SEIG design is 7.22%, which is lower compared to previous models.

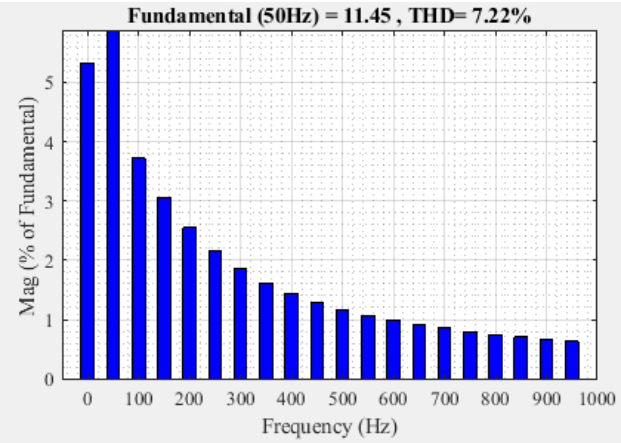

Figure 9 Analysis of total harmonic distortion.

MMF Plots and harmonics for model 1

The MMF which is normalized for its maximum value having 36 slots. **Figure 10** shows the MMF waveform for main winding. The winding configuration (**Table1**) for model 1 shows the magnitude response of electrical harmonic as shown in **Figure 11**. The 1st, 3rd and 5th harmonics are 1.0, 0.075 and 0.060, respectively.

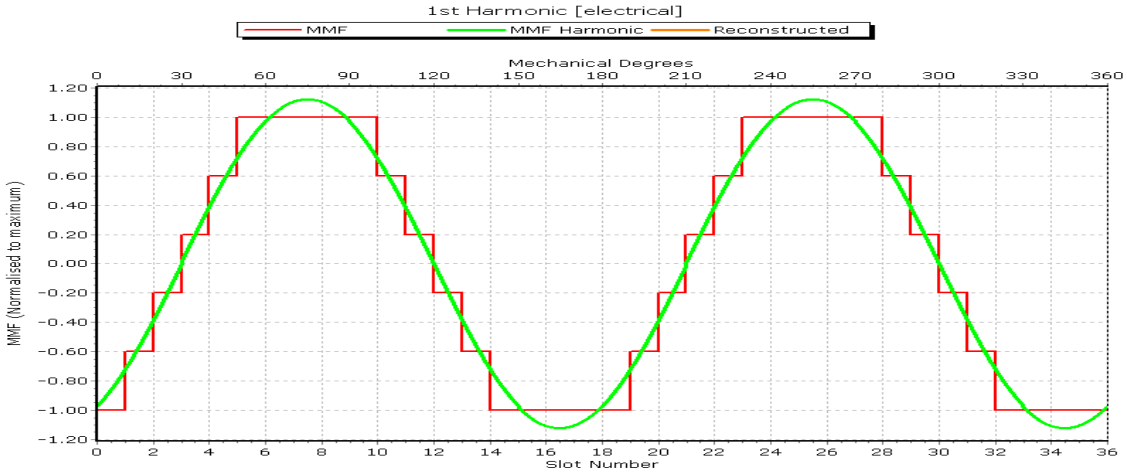

Figure 10 MMF plot for main winding.

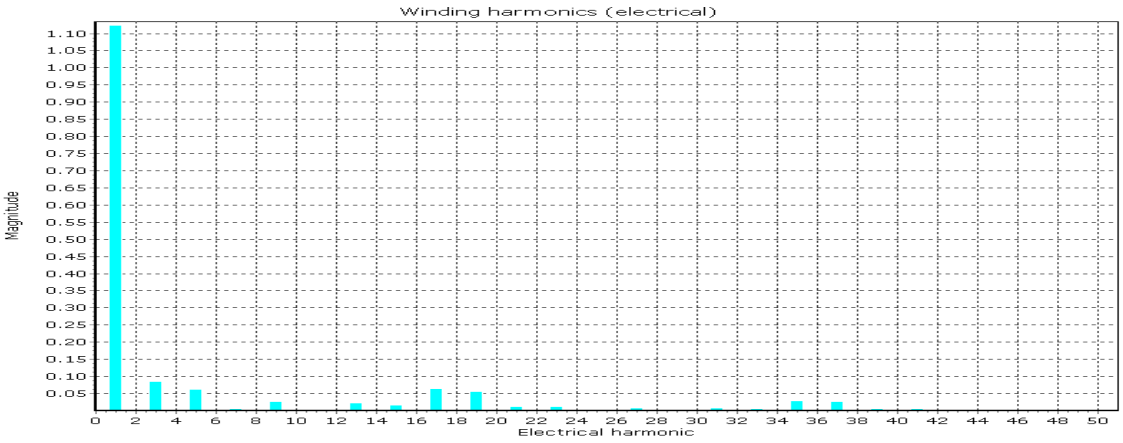

Figure 11 Harmonics plot model 1.

MMF Plots and harmonics for model 3

The MMF which is normalized for its maximum value having 36 slots. **Figure 12** shows the MMF waveform for main winding. The winding configuration (**Table 3**) for model 1 shows the magnitude response of electrical harmonic as shown in **Figure 13**. The 1st, 3rd and 5th harmonics are 1.0, 0.040 and 0.010, respectively. It is observed that, this is the lowest and optimum value of the electrical harmonic's comparative to other designed models.

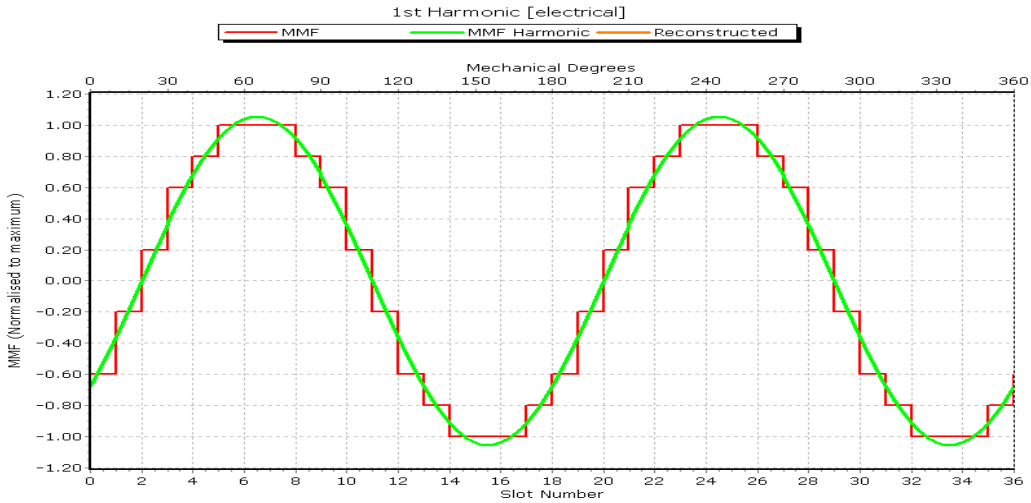

Figure 12 MMF Plot for main winding.

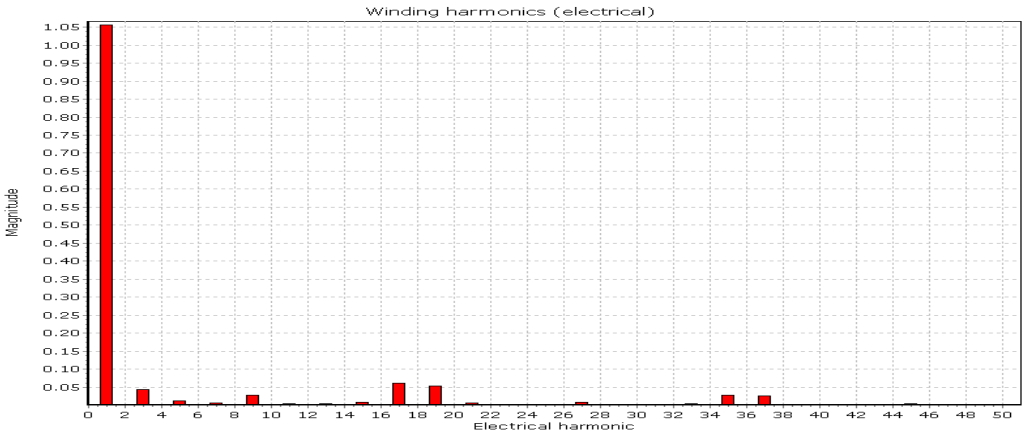

Figure 13 Harmonics plot model 3.

Conclusions

Two torque SEIGs at 220/230 V were provided by Matlab simulations and experimental tests, complete modeling and dynamic performance analysis of the same phase. The proposed model is reasonable to evaluate the performance of the generator under uniform or unbalanced load conditions. A brief overview and selection criteria of the induction generator design parameters of SEIG's single-phase machine theory are presented. When evaluating its output with different kinetic parameters, torque, speed, etc., the optimal trigger potential is evaluated for the SEIG. With the invention of the test layout, the design has been shown to be valuable for efficient performance. With changes in excitement and prime mover rate, the SEIG output varies considerably. Therefore, the performance analysis results show the effectiveness of the SEIG design. On comparing the performance of the 4 models, it has been observed that the model "Short pitch(1-8) Double layer winding" gives good performance in terms of reduced THD, sinusoidal MMF waveforms. Therefore, the finalized model is "Short pitch(1-8) Double layer winding" for a significant application in field. The main objective function is to minimize THD as well as pure sinusoidal waveform using design package SPEED.The objective function is achieved by suitable arrangement of winding specification.

References

[1] RK Jardan, P Stumpf, Z Varga and I Nagy. Novel solutions for high-speed self-excited induction generators. *IEEE Trans. Ind. Electron.* 2015; **63**, 2124-32.

[2] KS Sakkoury, S Emaraand MK Ahmed. Analysis of wind driven self-excited induction generator supplying isolated DC loads. *Int. J. Electron. Syst. Inform. Technol.* 2017; **4**, 257-68.

[3] UK Kalla, B Singh and SS Murthy. Intelligent neural network-based controller for single-phase wind energy conversion system using two winding self-excited induction generator. *IEEE Trans. Ind. Inform.* 2016; **12**, 1986-97.

[4] A Upasan and Y Kumsuwan. Closed loop speed control of induction generator with scalar-control inverters.*Int. J. Energy Proc.*, 2013; **34**, 371-81.

[5] NA Iqteit and AK Daud. A new model of self-excited induction generator to feed a single phase load with an application in lighting animal farm.*Int. J. Power Energy Convers*. 2019; **10**, 32-50.

[6] CP Ion and I Serban. Self-excited induction generator based microgrid with super capacitor energy storage to support the start-up of dynamic loads.*Int. J. Adv. Electron. Comput. Eng.* 2018;**18**, 51-61.

[7] K Makowski and A Leicht. Behaviour of single-phase self-excited induction generator during short-circuit at terminals. *Int. J. Comput. Math.Electr.Electron.Eng.*2018; **37**, 1815-23.

[8] K Makowski and A Leicht. Comparative analysis of single-phase self-excited induction generators of various rotor cages.*Int. J. Electron. Eng.*2019; **101**, 805-12.

[9] P Mehta, P Bhatt and V Pandya. Optimized coordinated control of frequency and voltage for distributed generating system using Cuckoo Search Algorithm.*Ain Shams Eng. J.* 2018; **9**, 1855-64.

[10] UK Kalla, B Singh and SS Murthy. Green controller for efficient diesel engine driven single-phase SEIG using maximum efficiency point operation. *IEEE Trans. Ind. Electr*on. 2016; **64**,264-74.

[11] UK Kalla,B Singhand SS Murthy. Modified electronic load controller for constant frequency operation with voltage regulation of small hydro-driven single-phase SEIG.*IEEE Trans. Ind. Appl*.2016;**52**, 2789-800.

[12] AS Satpathy, D Kastha and K Kishore. Control of a STATCOM-assisted self-excited induction generator-based WECS feeding non-linear three-phase and single-phase loads. *IET Power Electron.* 2018; **12**, 829-39.

[13] LG Scherer, RV Tambara and RF de Camargo. Voltage and frequency regulation of standalone self-excited induction generator for micro-hydro power generation using discrete-time adaptive control.*IET Renew. Power Gener.* 2016; **10**,531-40.

[14] UK Kalla, B Singh and SS Murthy. Slide mode control of microgrid using small hydro driven single-phase SEIG integrated with solar PV array.*IET Renew. Power Gener.* 2017; **11**, 1464-72.

[15] Y Zidani, S Zouggarand A Elbacha. Steady-state analysis and voltage control of the self-excited induction generator using artificial neural network and an active filter. *Iran. J. Sci. Technol. - Trans. Electr. Eng.* 2018; **42**, 41-8.

[16] H Arabaci. An iterative solution approach for steady state analysis of self-excited induction generator. *Int. J. Intell. Eng. Inform.* 2019; **7**, 309-22.

[17] M Arbi, K Marwa, BS Mouldi and BFH Rhaoulia. Performance evaluation of self-excited DSIG as a stand-alone distributed energy resources. *Int. J. Electr. Eng.* 2016; **98**, 159-67.

[18] SMS Salem. Study of wind turbine based self-excited induction generator under nonlinear resistive loads as a step to solve the Egypt electricity crisis.*Int. J. Electr. Comput. Eng.* 2016; **51**,1-11.

[19] AS Kumar, J Munda and G Singh. Wind-driven stand-alone six-phase self-excited induction generator transients under different loading conditions.*Int. J. Electr. Eng.* 2015; **97**.

[20] LG Scherer, CB Tischer and RF de Camargo. Power rating reduction of distribution static synchronous compensator for voltage and frequency regulation of stand-alone self-excited induction generator.*Int. J. Electr. Power Syst. Res.* 2017; **149**, 198-209.

[21] MM Basic and D Vukadinović. Online efficiency optimization of a vector controlled self-excited induction generator. *IEEE Trans. Energy Convers.* 2015; **31**, 373-80.

[22] FD Wijaya and H Prabowo. Voltage control of single-phase two winding self excited induction generator using SVC-MERS for isolated system. *Int. J. Power Electron. Drive Syst.* 2016;**7**, 901.

[23] WE Vanco, FB Silva, FA Goncalves and CA Bissochi. Evaluation of the capacitor bank design for self-excitation in induction generators. *IEEE Lat. Am. Trans.* 2018; **16**, 482-8.

[24] HM Hasanien and GM Hashem. A cuckoo search algorithm optimizer for steady-state analysis of self-excited induction generator. *Ain Shams Eng. J.* 2018; **9**, 2549-55.

[25] LG Scherer, RV Tambara and RFD Camargo. Voltage and frequency regulation of standalone self-excited induction generator for micro-hydro power generation using discrete-time adaptive control. *IET Renew. Power Gener.* 2016; **10**, 531-40.

[26] UK Kalla, B Singh and SS Murthy. Intelligent neural network-based controller for single-phase wind energy conversion system using two winding self-excited induction generator. *IEEE Trans. Ind. Inform*. 2016; **12**, 1986-97.

[27] A Krishnan, K Anusha, N Kumaresan and S Senthil Kumar. Simplified methods for the analysis of self-excited induction generators. *IET Electr. Power Appl.* 2017; **11**, 1636-44.

[28] SS Murthy, B Singh and VSandeep. Experience in developing a single-phase two winding 5 kW self-excited induction generator for off-grid renewable energy based power generation. *J. Inst. Eng. (India): B*. 2016; **97**, 127-37.

[29] LG Scherer, CB Tischer and RFD Camargo. Power rating reduction of distribution static synchronous compensator for voltage and frequency regulation of stand-alone self-excited induction generator. *Electr. Power Syst. Res.* 2017; **149**, 198-209.